Supplementary Information (SI) for New Journal of Chemistry.

Supporting Information

1. UV- reflectance spectroscopy

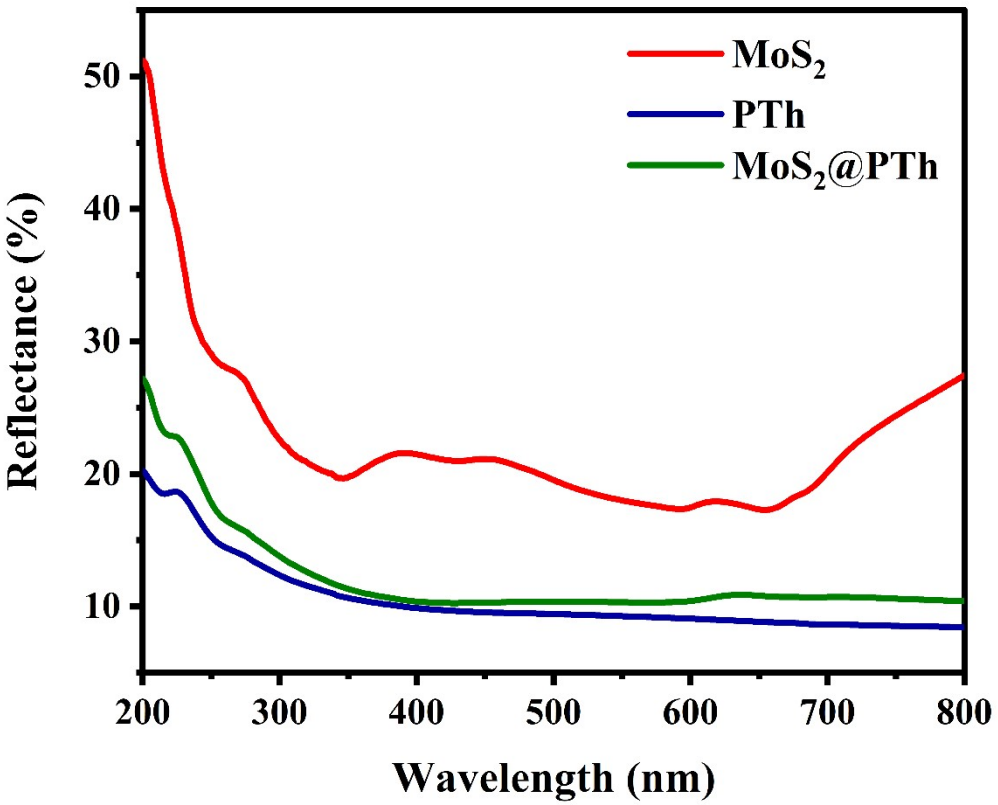

Fig. S1 Reflectance spectra of prepared photocatalyst PTh, MoS_2 and MoS_2@PTh

2. Photocatalytic Hydroxyl Radicals (•OH) Production

To further verify the generation of hydroxyl radicals (•OH) during the photocatalytic process, coumarin was employed as a selective fluorescent probe. In a typical experiment, 30 mg of the nanocatalyst was introduced into the coumarin solution and stirred vigorously under the same reaction conditions used for the degradation studies. Upon light irradiation, coumarin interacts specifically with •OH to yield 7-hydroxycoumarin, a highly fluorescent compound. The formation of 7-hydroxycoumarin is evidenced by its distinctive optical characteristics, showing an excitation peak at 334 nm and a strong emission band around 426 nm. During irradiation, the fluorescence intensity at 426 nm increased steadily with reaction time. This

continuous rise in emission signifies a proportional increase in •OH formation, indicating that the photocatalyst produces hydroxyl radicals efficiently throughout the reaction period. These observations corroborate the radical-scavenging results and provide convincing evidence that •OH radicals act as the principal reactive species responsible for driving the photocatalytic degradation of the targeted pollutants. Thus, the coumarin fluorescence assay strongly supports the proposed reaction mechanism and highlights the crucial contribution of hydroxyl radicals in the overall catalytic activity.

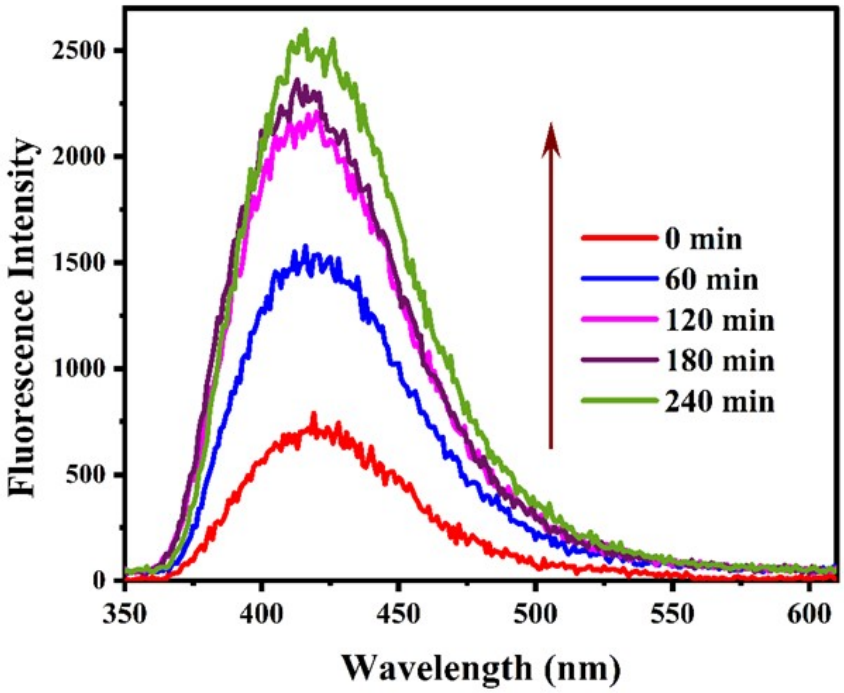

Fig. S2. Fluorescence spectral changes of coumarin solution monitored at 425 nm during irradiation with a 150 W visible-light source, recorded in a 2.5 µM aqueous coumarin solution

3. EIS analysis

Electrochemical impedance spectroscopy (EIS) was performed to evaluate the charge transfer behavior of PTh, MoS_2, and the MoS_2@PTh nanocomposite. In the Nyquist plots, a smaller semicircle diameter corresponds to lower charge transfer

resistance, indicating more efficient charge separation and improved interfacial charge mobility. The semicircle radii followed the order PTh > MoS_2 > MoS_2@PTh, confirming that the composite exhibits significantly reduced electron transfer resistance and suppressed electron–hole recombination. Among all samples, MoS_2@PTh displayed the smallest arc radius, demonstrating superior electrical conductivity and accelerated charge transport, which is consistent with the PL analysis indicating enhanced charge separation efficiency.

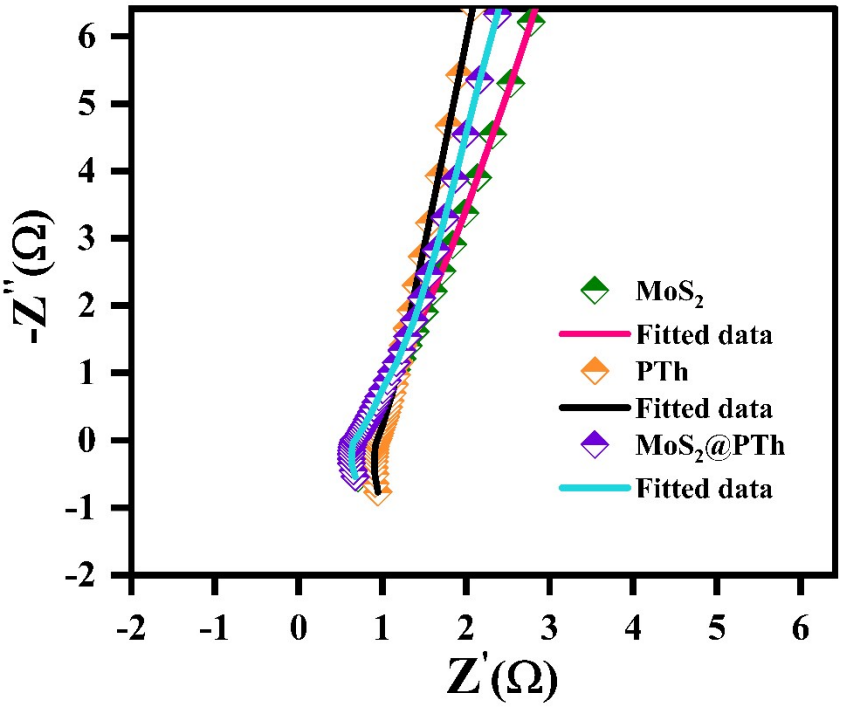

Fig. S3. Electrochemical impedance spectroscopy of PTh, MoS_2 and MoS_2@PTh

3.5. Intermediate product analysis and toxicity assessment

The photocatalytic degradation of ciprofloxacin (CIP) and tetracycline (TC) and over MoS_2@PTh was investigated using LC–MS analysis. This technique enabled the identification of major intermediate products and the proposal of plausible degradation pathways based on the detected mass spectral signals and previously reported literature

[1,2,3,4]. The prominent intermediate products observed in the mass spectra were characterized by m/z values of 304, 292.1, 244, 232.8, 184.8, 135, and 102.8.

Ciprofloxacin (CIP, m/z = 332) undergoes photocatalytic degradation through a series of reactions including oxidation, N-dealkylation, hydroxylation, defluorination, and ring-cleavage processes [5]. In the initial degradation route (Pathway I), the parent ion (m/z = 332) undergoes oxidative decarboxylation with the loss of the $–CO_2$ group, forming an intermediate at m/z = 304 [6,7]. Subsequent removal of the $–CH_3CH_2N$ moiety from the piperazine ring produces a fragment ion at m/z = 244.8. Further attack by reactive oxygen species (•OH and $•O_2^-$) induces N-dealkylation, generating intermediate C2 (m/z = 244), followed by piperazine ring cleavage to form intermediate C3 (m/z = 198) [6]. The fragment ion at m/z = 232.8 is attributed to the loss of a $–CH_2$ group from the residual piperazine ring, which subsequently undergoes complete ring elimination to produce an ion at m/z = 184.4 [7].

In Pathway II, CIP initially undergoes the simultaneous removal of the $–CH_2CH_2NH–$ group from the piperazine ring and decarboxylation ($–CO_2$), yielding an intermediate at m/z = 244.9. This intermediate follows a degradation route similar to that observed in Pathway I. Continued oxidation and ring-opening reactions mediated by •OH and $•O_2^-$ radicals result in the formation of low-molecular-weight intermediates, including C_5 at m/z = 102.8, indicating extensive mineralization of the ciprofloxacin molecule. To further evaluate the major tetracycline (TC) degradation intermediates identified in Fig. S4b, LC–MS analysis was employed during the photocatalytic degradation of TC (m/z = 444). The results indicate that reactive oxygen species (ROS), particularly hydroxyl radicals (•OH) and superoxide radicals ($•O_2^-$), play a dominant role in initiating a series of oxidative transformations that lead to the progressive structural breakdown of the TC molecule [6,7,8,9,10]. The degradation of TC proceeds mainly through two principal pathways. In Pathway I, superoxide radicals ($•O_2^-$) preferentially attack the electron-rich regions of the TC molecule, resulting in the formation of intermediate T_1 (m/z=263)[6]. This transformation involves multiple reactions, including dihydroxylation, deamination, oxidative decarboxylation, C–C

bond cleavage, and hydroxylation. Subsequently, the loss of hydroxyl groups and molecular rearrangement of T_1 leads to the formation of T_2 (m/z = 242). Further decarboxylation and hydroxylation reactions convert T_2 into T_3 (m/z = 198).

With continued exposure to the oxidative ROS environment, successive removal of hydroxyl (–OH) and carboxyl (–COOH) functional groups results in the formation of lower-molecular-weight intermediates at m/z = 155 and T_4 (m/z = 123). Progressive dealkylation, demethylation, and oxidation reactions further break down these intermediates into smaller fragments (m/z = 122). Ultimately, these low-molecular-weight products undergo complete oxidation to CO_2 and H_2O, indicating near-complete mineralization of TC under the applied photocatalytic conditions.

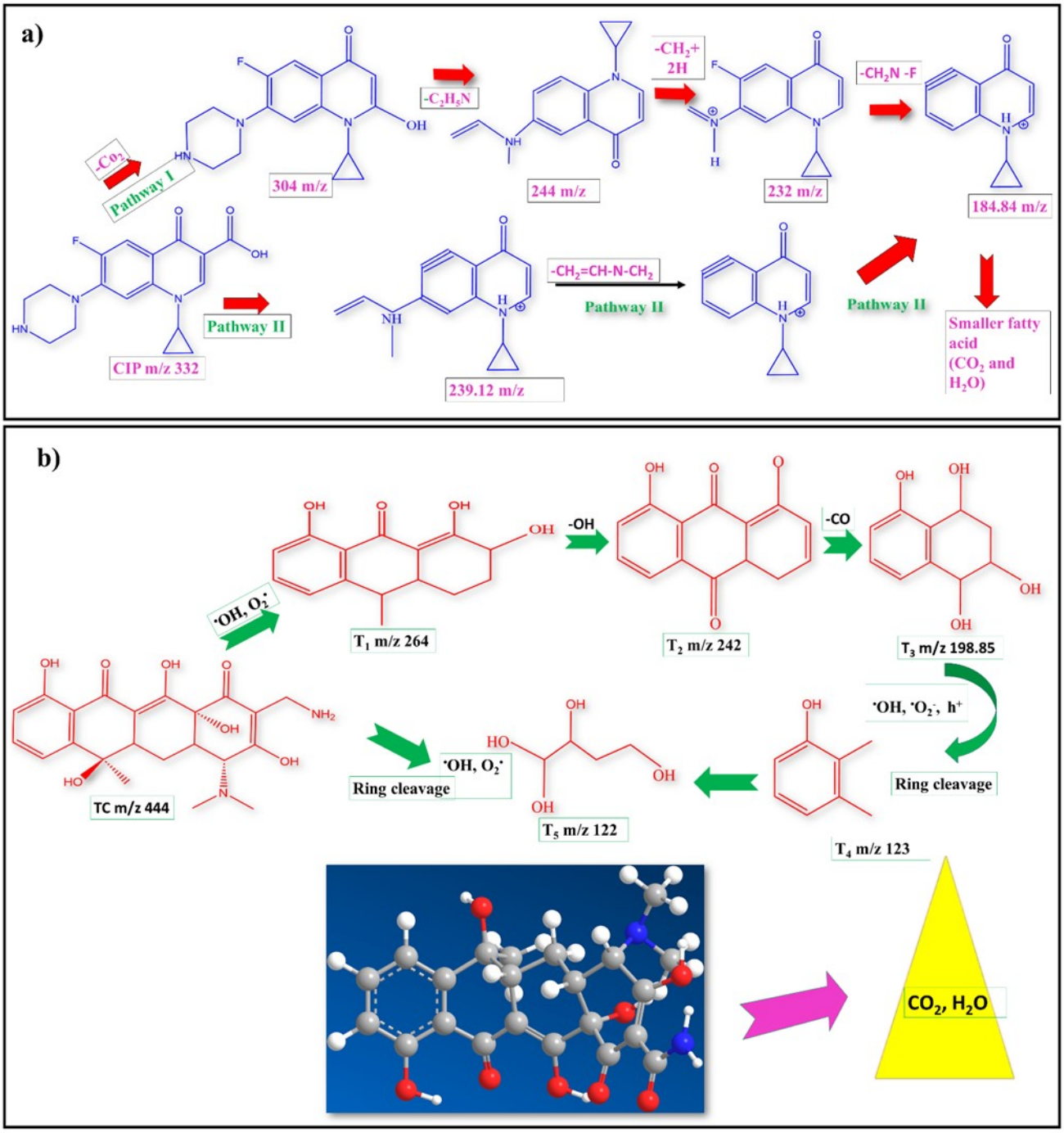

Fig. S4. Plausible LC–MS-based degradation pathway of ciprofloxacin (CIP) and tetracycline (TC) over MoS_2@PTh,

In the case of RhB, LC–MS analysis was employed to monitor the temporal evolution of intermediate species formed during photocatalytic degradation, thereby providing insights into the possible degradation pathways. The corresponding LC–MS spectra of RhB after 240 min of visible-light irradiation in the presence of MoS_2@PTh

are presented in Fig. S5. As shown in this figure, characteristic m/z peaks at 443, 387.93, 318.41, 184.84, and 166.60 were clearly detected, corresponding to the parent RhB molecule and its degradation intermediates,. the dominant peak at m/z = 443 corresponded to intact RhB, accompanied by the formation of N,N-diethyl rhodamine at m/z = 387.93. This observation indicates that the degradation of RhB is initiated by a stepwise N-deethylation process, involving the successive removal of ethyl groups (–C_2H_5) from the diethylamino substituents. Such deethylation reactions are widely recognized as the primary degradation pathway of RhB under photocatalytic conditions. With prolonged irradiation, additional lower-molecular-weight intermediates at m/z = 318.41, 184.84, and 166.60 appeared, suggesting that the chromophore ring underwent further oxidative cleavage. Following N-desethylation, the resulting intermediates were further degraded into lower m/z species. Oxidative chromophore cleavage converted these intermediates into small carboxylic acids, including phthalic acid and terephthalic acid (m/z = 166), and adipic acid (m/z = 146)[11-13].These transformations are mainly driven by highly reactive oxygen species (ROS), particularly hydroxyl radicals (•OH) and superoxide radicals ($\bullet O_2^-$) generated on the MoS_2@PTh photocatalyst under visible-light excitation. The •OH radicals, owing to their strong oxidative potential, play a dominant role in promoting hydrolysis, oxidation, and ring-opening reactions, leading to the breakdown of the conjugated xanthene structure [14]. Meanwhile, $\bullet O_2^-$ contributes to the oxidation of intermediate species and facilitates subsequent molecular fragmentation. Additionally performed LC–MS analysis of Brilliant Blue degradation over MoS_2@PTh revealed intermediate ions at m/z 390.43, 343.40, 224.36, and 222.87, indicating stepwise oxidative fragmentation of the dye molecule. The initial degradation involved cleavage of the triphenylmethane chromophore and desulfonation, producing a major intermediate at m/z 390.43. Subsequent hydroxyl radical attack led to further aromatic ring degradation, yielding the m/z 343.40 fragment. Advanced oxidation resulted in low-molecular-weight aromatic intermediates at m/z 224.36 and 222.87, confirming deep degradation and progressive mineralization of Brilliant Blue.

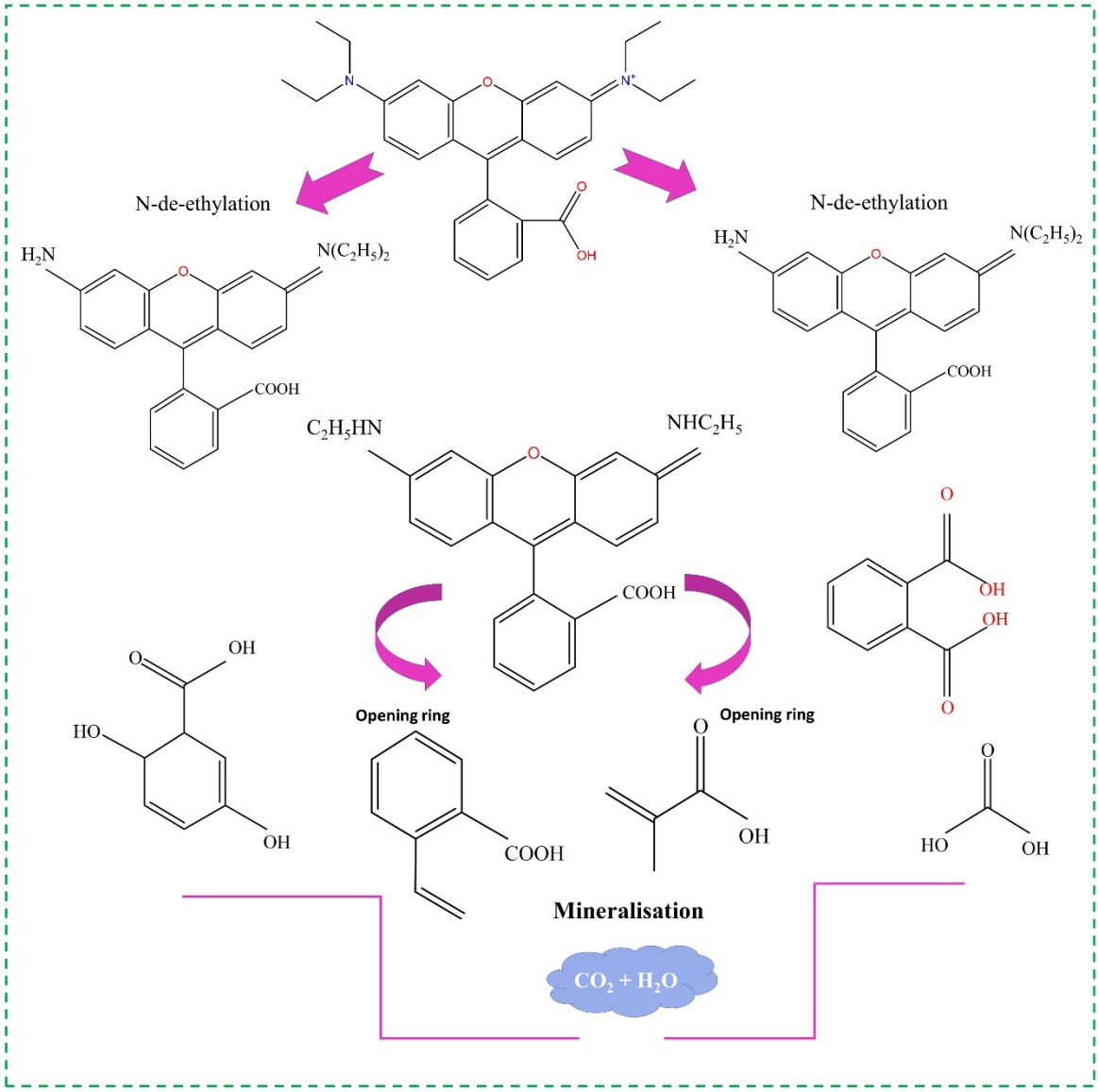

Fig. S5 Possible degradation pathway for degradation of Rhodamine B

References

1. He, Z., Shi, T., Chen, D., Wang, Y., Feng, Y., Zhou, F. and Li, Y., 2025. Ultrathin CuZnCr-LDH nanosheets for photo-Fenton synergistic degradation of ciprofloxacin and methylene blue. Journal of Alloys and Compounds, 1010, p.177302.CIP

2. Liu, X., Chen, S., Tantai, X., Dai, X., Shao, S., Wu, M., Sun, P. and Dong, X., 2025. Regulating defects in sulfur-doped Bi4O5I2 and constructing S-scheme heterojunctions with g-C3N4 to enhance photocatalytic antibiotic degradation. Separation and Purification Technology, 363, p.132001. TC

3. Cai, Z., Xia, W., Li, H., Qin, R., Wu, F., Wu, J., Yin, X., Li, Z. and Yang, Y., 2024. Mg-Doped ZnO-PVDF Composite Membranes by Interfacial Film-Forming Method for Adsorption and Piezoelectric Degradation of Tetracycline in Water. ACS Applied Polymer Materials, 6(12), pp.7171-7183.

4. Lakshmi, C.N., Irfan, M., Sinha, R. and Singh, N., 2024. Magnetically recoverable Ni-doped iron oxide/graphitic carbon nitride nanocomposites for the improved photocatalytic degradation of ciprofloxacin: Investigation of degradation pathways. Environmental Research, 242, p.117812. CIP

5. Verma, A., Priyadarshini, U. and Remya, N., 2025. Solar photocatalytic degradation of ciprofloxacin using biochar supported zinc oxide-tungsten oxide photocatalyst. Environmental Science and Pollution Research, 32(15), pp.9412-9428.

6. Bharathi, A.M., Neppolian, B. and Krishnamurthi, T., 2025. Enhanced molecular oxygen activation via Z-scheme $Bi_2MoO_6/Bi_4Ti_3O_{12}$ heterojunction for photocatalytic degradation of tetracycline and ciprofloxacin: Performance and intermediate toxicity appraisement. Journal of Environmental Chemical Engineering, p.118047.

7. Mai, N.T., Van Thanh, D., Huy, N.N., Bich, D.D., Hang, T.T.M., Hao, N.H. and Khai, N.M., 2025. Red mud supported on rice husk biochar as sono-photo-Fenton catalysts for degradation of ciprofloxacin in water. Separation and Purification Technology, 354, p.129039.

8. Sun, X., Wang, T. and Yun, S., 2023. Construction of 2D/2D g-C3N4@ Bim+ 1Fem-3Ti3O3m+ 3 (m= 4, 5, 6) S-scheme heterojunctions for efficient photocatalytic tetracycline degradation. Journal of Materials Research, 38(11), pp.2943-2957.

9. Guo, R., Zhong, Y., Wang, B., Li, L., Qin, W., Tan, Y., Zhao, Z., Liu, N. and Mo, Z., 2025. Efficient photocatalytic degradation of tetracycline and its derivatives by green recyclable PAN/Bi2WO6/Cu2O nanofiber membrane. Separation and Purification Technology, 358, p.130239.

10. Zhou, P., Han, X., Wu, L., Qi, M., Shen, Y., Nie, J., Liu, X., Wang, F., Bian, L. and Liang, J., 2025. Facile construction of novel BiOBr/black-TiO2/tourmaline composites for the synergistic degradation of tetracycline in aqueous. Separation and Purification Technology, 362, p.131976.

11. Bikerchalen, S., Mllaoiy, L., Saddik, N., Bakiz, B., Villain, S., Taoufyq, A., Guinneton, F., Valmalette, J.C., Gavarri, J.R. and Benlhachemi, A., 2025. Optimization of solvothermal synthesis parameters for Bi24O31Cl10: Enhanced photocatalytic performance, degradation pathways, and mechanism of organic pollutants. Journal of Physics and Chemistry of Solids, p.113267.

12. Bouddouch, A., E. Amaterz, B. Bakiz, F. Guinneton, A. Taoufyq, S. Villain, J-R. Gavarri, M. Mansori, J-C. Valmalette, and A. Benlhachemi. "High photocatalytic performance of bismuth phosphate and corresponding photodegradation mechanism of Rhodamine B." *Research on Chemical Intermediates* 48, no. 8 (2022): 3315-3334.

13. Shalinibabu, C., Pattar, M., Nagaraja, K.K. and Pramodini, S., 2026. Zinc oxide assisted photocatalytic degradation of mixed effluents of rhodamine B dye and paracetamol drug mediated by acid blue 25 dye. Journal of Water Process Engineering, 81, p.109272.

14. Bikerchalen, S., Akhsassi, B., Bakiz, B., Villain, S., Taoufyq, A., Guinneton, F., Gavarri, J.R. and Benlhachemi, A., 2025. Photocatalytic degradation of Rhodamine B dye over oxygen-rich bismuth oxychloride Bi24O31Cl10 photocatalyst under UV and visible light irradiation: pathways and mechanism. Journal of Physics and Chemistry of Solids, 196, p.112342.